Femtosecond laser direct writing multilayer chiral waveplates with minimal linear birefringence

JIAFENG LU,[1,2] ENRIQUE GARCIA-CAUREL,[3] RAZVIGOR OSSIKOVSKI,[3] FRANCOIS COURVOISIER,[4] XIANGLONG ZENG,[2] BERTRAND POUMELLEC,[1] MATTHIEU LANCRY[1,*]

[1] *Institut de Chimie Moléculaire et des Matériaux d'Orsay, Université Paris Saclay, Orsay cedex 91405, France*
[2] *The Key Lab of Specialty Fiber Optics and Optical Access Network, Joint International Research Laboratory of Specialty Fiber Optics and Advanced Communication, Shanghai University, Shanghai 200444, China*
[3] *LPICM, CNRS, Ecole Polytechnique, Institut Polytechnique de Paris, Palaiseau 91128, France*
[4] *FEMTO-ST Institute, University Bourgogne Franche-Comté, CNRS, Besançon 25030, France*
[*] *Corresponding author: matthieu.lancry@universite-paris-saclay.fr*

Chirality transfer from femtosecond laser direct writing in achiral transparent materials mainly originates from the interplay between anisotropic nanogratings and mechanical stress with non-parallel and non-perpendicular (oblique) neutral axes. Yet, the laser fabrication simultaneously induces non-negligible linear birefringence. For precise manipulation of circular polarization properties, as well as to unlock the full functionality, we report here a geometry-inspired multilayer method for direct writing of chiral waveplates with minimal linear birefringence. We perform a theoretical analysis of both circular and linear properties response for different multilayer configurations and achieve strong circular birefringence of up to -2.25 rad with an extinction ratio of circular birefringence to total linear birefringence of up to 5.5 dB at 550 nm. Our strategy enables the precise control of circular properties and provides a facile platform for chiral device exploration with almost no linear property existence.

Chiral effects originating from diverse phenomena in nature have shown their great importance both in fundamental science and in practical applications ranging from molecular chemistry to artificial metamaterials, such as optical recording [1], broadband circular polarizers [2] and quantum materials [3]. Chiral structures mix electric and magnetic contributions, originating in different optical responses to left- and right- handed circular polarized light. Thus, a chiral waveplate (like, e. g. water solution of sugar) enabling pure optical rotation without ellipticity is very useful. Compared to traditional optical rotators, such as half-waveplates that require very precise retardance and alignment and Faraday rotators that require complex devices, chiral waveplates exhibit compact sizes, are less sensitive to misalignment and are potentially achromatic [4].

Femtosecond (fs) laser direct writing (FLDW) is an alternative photonic device fabrication strategy, which, in recent years, has evolved from the proof-of-principle stage to a widely exploited procedure in optical manufacturing [5]. Due to its ultrahigh peak power and ultrashort pulse duration, a fs laser can locally deposit the energy in the irradiated region without any surrounding damage through nonlinear effects [6]. This subsequently results in diverse kinds of nanostructures. Among these, Type II structures (subwavelength nanogratings), consisting of an alternation of nanoporous layers, exhibit strong symmetry breaking [7–10]. In general, this gives rise to linear polarimetric properties, such as dichroism and birefringence [11]. Going a step further, the use of a fs laser to induce circular properties inside achiral materials opens up interesting perspectives for creating chirality in three-dimensional structures, which is the key step in fabricating chiral transparent waveplates [12]. Physically, the fs-laser-induced chirality was attributed to a volume torque resulting from a DC electric field and a stress field [12]. However, the changes in molecular configuration taking place in such an ultrashort light-matter interaction are difficult to observe. In a recent work, we proposed a new conceptual view according to which fs-induced circular properties are due to two main contributions: a form birefringence due to nanogratings and a photoelastic birefringence originating from stress with oblique neutral axes [13].

A typical fs-laser-written chiral structure exhibits strong linear birefringence due to the anisotropic structure of nanogratings [14,15], restricting the performance of the chiral waveplate (because of linear birefringence transforming linearly polarized light into elliptically polarized one). Recently, Yoo et al. [16] reported that birefringent tapes stacked in multilayers with appropriate azimuth orientations (best results with $45°$ difference between the layers having been obtained) can create circular properties with suppressed linear properties. Following this conceptual view, here we go a step further in imprinting directly a chiral waveplate structure with linear properties suppression by utilizing a multilayer stack configuration through FLDW.

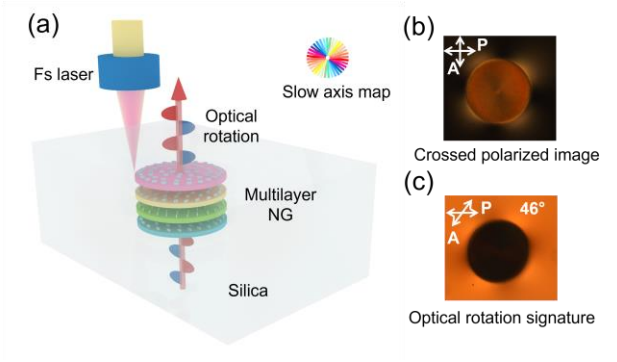

Fig. 1. (a) Scheme of the fs-laser-written structure consisting in layers of nanogratings with different slow axis orientations that lead to large optical rotation. The inset shows the map of the slow axis orientation, different colors corresponding to different slow axis orientations. (b) Cross-polarized microscope image of a four-layer sample written at 1030 nm, 800 fs, 0.16 NA, 100 kHz, 0.8 μJ, 1 mm/s, $\alpha = 45°$. (c) Optical rotation signature obtained with the analyzer in extinction configuration. This measurement confirms that the polarization remains linear, with an azimuth rotated by 46° with respect to the incident polarization.

Fs-laser-enabled writing of oriented multilayer assemblies is based on the neutral axis (typ. slow/fast axis in uniaxial materials) control of imprinted nanogratings by exploiting appropriate laser parameters such as laser polarization, as illustrated in **Fig. 1(a)**. In this paper, we adopt a four-layer configuration as an easy-to-obtain yet a practically useful design. Actually, four layers with rotated slow axis orientation angles (azimuths) create a staircase-like configuration resulting in strong chiral effects. Here, the increment angle α is defined as the angle between the slow axis directions of two adjacent layers. For simplicity, identical retardation for all layers is assumed and the increment angle α is kept constant in one single configuration.

The fs-laser system (Amplitude Systèmes, Pessac, France) delivers a laser beam at the wavelength $\lambda = 1030\ nm$ with an 800-fs duration time. A 100-kHz repetition rate with pulse energy in the 0.6-2.0 μJ range was used for the fabrication of Type II nanogratings. A low numerical aperture (0.16 NA) aspheric lens was used to minimize spherical aberration. We fabricated several mm-size disks using a spiral writing trajectory with an increment of 1 μm in order to ensure homogeneity and suppress diffraction. More information can be found in [13]. The samples were fabricated through irradiation of a 1-mm thick silica glass wafer (Suprasil CG, Heraeus, Hanau, Germany) by focusing the laser beam 400 μm below the surface. (The latter value corresponds to the deepest layer when in a multilayer configuration.) Based on preliminary calibrations, the laser parameters used were set at appropriate pulse energies and scanning speeds to ensure the fabrication of well-controlled Type II nanogratings.

We start with the increment orientation angle $\alpha = 45°$ inspired by the reported work from Yoo et al. [16]. **Figures 1(b)** and **1(c)** show the cross-polarized microscope image and the optical rotation signature (obtained with the analyzer in extinction configuration) of a four-layer sample, exhibiting a large optical rotation of up to $46°$. The optical microscope images were recorded with an Olympus BX51 polarizing optical microscope equipped with a "de Sénarmont" compensator. This configuration not only enables the optical rotation measurement with a high precision 180-degree-rotation analyzing polarizer but also enables a linear retardance measurement with an accuracy of few nanometers at 550 nm by employing a highly precise quarter-waveplate.

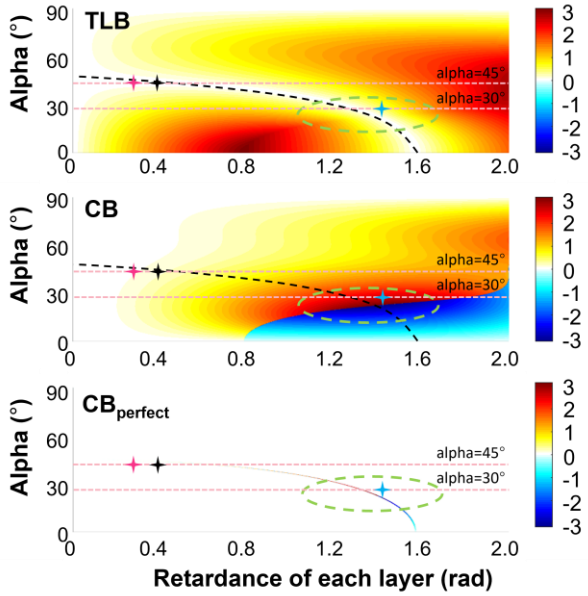

Fig. 2. Modeling results of four-layer staircase-like structures at different increment angles α and retardances. Top figure: TLB (total linear birefringence); Center figure: CB (circular birefringence); Bottom figure: $CB_{perfect}$ (CB values from the black dashed line). Black dashed line: zero-TLB curve; Red star: structure from Yoo et al. [16]; Black star: sample written by 0.8 μJ, 1 mm/s, $\alpha = 45°$; Blue star: sample written by 1.5 μJ, 1 mm/s, $\alpha = 30°$; Green dashed line region: chiral waveplates with strong CB and significantly small TLB.

The optical rotation signature originates not only from the chiroptic properties of each individual layer but also from the azimuth misalignment between layers. The thicker each layer, the higher the retardance (optical phase difference). The thickness of a single layer was measured to be around 40 μm and the distance between two adjacent layers was set to 100 μm, effectively allowing for stress uncoupling between layers. We have theoretically modeled the chiroptic properties of a four-layer configuration nanogratings-based waveplate using Mueller matrix formalism. Theoretically, the optical response of an individual nanogratings layer is that of a linear retarder with a retardation R and a slow axis oriented at the angle α. Hence, the Mueller matrix of each layer can be expressed as: $M_{in}(R,\alpha) = MR(-\alpha) \cdot MLR(R) \cdot MR(\alpha)$,

$$MLR(R) = \begin{bmatrix} 1 & 0 & 0 & 0 \\ 0 & 1 & 0 & 0 \\ 0 & 0 & cos(R) & sin(R) \\ 0 & 0 & -sin(R) & cos(R) \end{bmatrix}$$

$$where \qquad MR(\alpha) = \begin{bmatrix} 1 & 0 & 0 & 0 \\ 0 & cos(2\alpha) & sin(2\alpha) & 0 \\ 0 & -sin(2\alpha) & cos(2\alpha) & 0 \\ 0 & 0 & 0 & 1 \end{bmatrix} \qquad (1)$$

We have set the same interlayer rotation angle. The final Mueller matrix of the chiral waveplate is given by:

$$M = M_{in4th}(R, 3\alpha) \cdot M_{in3rd}(R, 2\alpha) \cdot M_{in2nd}(R, \alpha) \cdot M_{in1st}(R, 0°) \quad (2)$$

The quantitative analysis of both linear and circular properties of the chiral waveplate is subsequently performed by applying the differential decomposition method [17,18]. The decomposed differential matrix is given by:

$$M_{dec} = \begin{bmatrix} 0 & LD & LD' & CD \\ LD & 0 & CB & -LB' \\ LD' & -CB & 0 & LB \\ CD & LB' & -LB & 0 \end{bmatrix} \quad (3)$$

Thus, we obtain the full set of optical properties: circular birefringence (CB), circular dichroism (CD), *x-y* axis linear birefringence (LB), 45°-axis linear birefringence (LB'), *x-y* axis linear dichroism (LD), and 45°-axis linear dichroism (LD'). The total linear birefringence (TLB) is determined from $TLB = \sqrt{LB^2 + LB'^2}$.

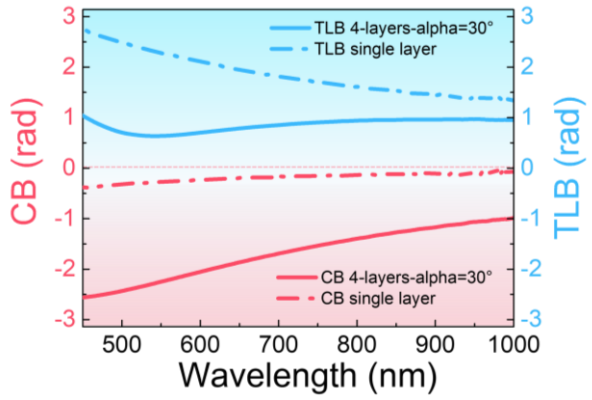

Fig. 3. CB and TLB wavelength dependence of the four-layer structure (solid lines) written at 1030 nm, 800 fs, 0.16 NA, 100 kHz, 1.5 µJ, 1 mm/s with an increment orientation angle α = 30°. Single-layer structure responses (dashed lines) with same laser parameters are reported for comparison.

Figure. 2 shows the modeling results of four-layer structures. Calculated TLB (top), CB (center) and $CB_{perfect}$ (bottom), i.e., CB values from the zero-TLB curve (black dashed line), as functions of *R* and α are shown. TLB is zero for certain pairs of *R* and α values (black dashed line). The model also shows that CB reaches the maximum value, close to ⍰, with still low TLB within the region bounded by the green dashed line. The latter region represents the most interesting configurations for practical applications.

To further explore the optical response of such chiral structures, we characterized them by spectroscopic Mueller ellipsometry and performed optical rotation measurements by cross-polarized microscopy. The normalized spectral Mueller matrix was first measured with a spectroscopic Mueller ellipsometer (Smart SE, JY HORIBA) and then decomposed with the differential decomposition method providing the matrix from **Eq. (3)**.

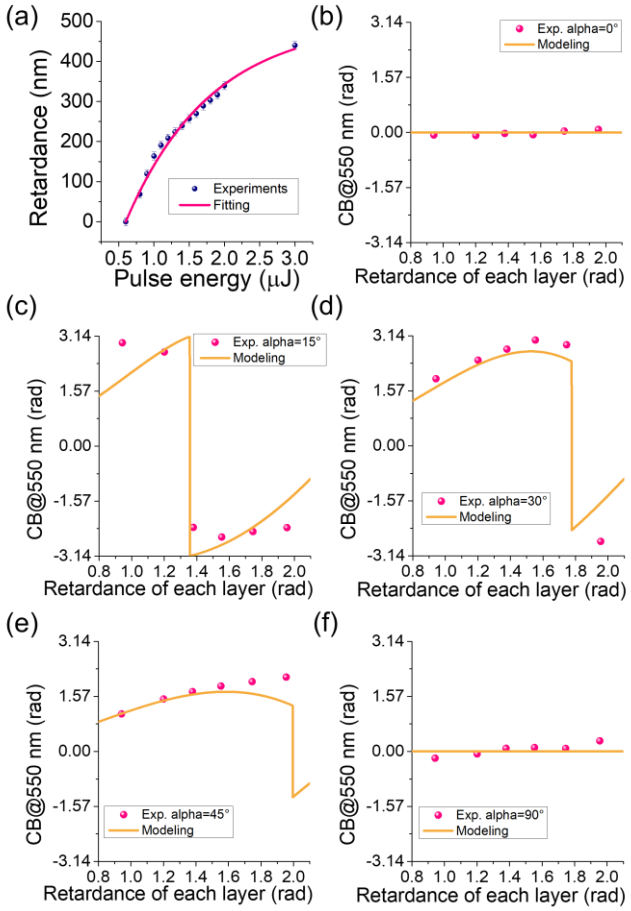

Fig. 4. (a) Experimental calibration results of retardance versus laser pulse energy. Experimental (points) and modeling (solid lines) results of four-layer structures with different orientation angle values versus retardance: $\alpha = 0°, 15°, 30°, 45°, 90°$ for (b)-(f), respectively.

The experimental CB and TLB spectroscopic dependence of the four-layer structure, as well as of a single layer structure given for comparison, are reported in **Fig. 3**. In order to reduce the impact of the mechanical stress resulting from the fs-laser-induced net volume expansion, the samples were annealed at 1125 °C for 30 minutes, a method proven to effectively relax the stress-induced birefringence [13]. The studied structure can thus be seen as a four-layers stack written at 1.5 µJ, 1 mm/s with an orientation difference angle α equal to 30°. Intuitively, such a staircase-like pile of layers acts somewhat similarly to a helix and exhibits remarkable CB values of up to -2.25 rad at 550 nm while the TLB value is only 0.64 rad. In contrast, a normal single layer structure written with the same parameters exhibits a very small CB of -0.27 rad but a high TLB value of 2.29 rad, as shown in **Fig. 3**. Our experimental approach thus demonstrates the ability of suppressing the TLB value while achieving high CB in a multilayer chiral waveplate. To quantify the performance of the chiral waveplate, we define an extinction ratio of CB to TLB as follows:

$$ER = 10 * Log(|CB|/|TLB|) \quad (4)$$

One obtains an ER of 5.5 dB at 550 nm for the chiral waveplate marked with the blue star located close to the center in the green dash line region in **Fig. 2**. One can still slightly tune the writing parameters and

optimize the assembly of multilayers to obtain an even higher ER value by reaching the center of the target region.

Regarding practical applications, one should consider the tailoring of chiral optical properties through simple writing parameters manipulation. Here, we utilize pulse energy as a parameter to tailor the optical properties profile of the multilayer structures. **Figure 4(a)** shows the single layer calibration result of the retardance (expressed in nanometers and related to TLB through $R/\lambda = TLB/\pi$) as a function of the laser pulse energy. We also explore the effect of the increment angle α between adjacent layers. **Figures 4(b-f)** show experimental data combined with modeling results of four-layer structures with different α versus the imprinted retardance. There are a few degrees (7°-8°) of deviation between the nominal and modeled values of α, tentatively attributed to a bias in the orientation of the slow axis of the nanogratings, which could be either due to the pulse front tilt (PFT) effect and/or the influence of the stress field on the nanolayers orientation [19]. Temporal and spatial chirps (caused by a slight misalignment of the laser compressor) can lead to PFT effect as investigated by Dai et al. [19]. After accounting for the deviation, we observe a quite good agreement between the experiment and the model for the CB evolution with retardance. Note that if one reduces the increment, the cumulative stress in the transition region cannot be ignored and will affect the chiroptic properties. Besides, if the increment is further reduced to an overlap of adjacent layers, or even continuous writing, the presence of transition regions should be considered, and the model should be refined. However, after having modeled different kinds of transition regions, we found that the staircase model of "independent" layers without transition regions described best our experimental results.

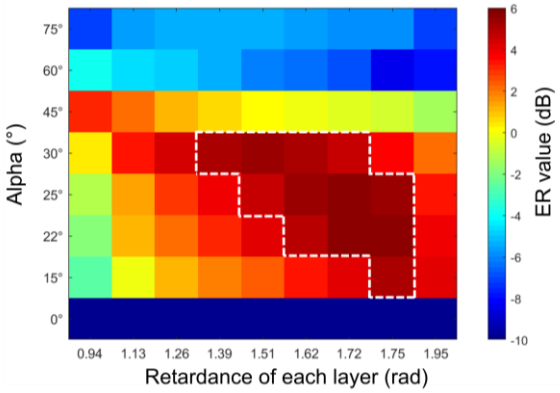

Fig. 5. (a) Experimental ER value map of four-layer structures for different orientation angle and retardance values. White dashed line region: the most interesting structures that exhibit ER values higher than 4.5 dB.

Next, we summarize the ER value map of the four-layer structures with different alpha and retardance values. It can be observed in **Fig. 5** that "$\alpha = 0°$" structures exhibit very small ER values (i.e., very small CB but large TLB) whatever the retardance value of the layers. Large ER values (higher than 4.5 dB as delimited by the white dash line) are found in structures with α ranging from 15° to 30° and an easy-to-obtain range of retardances. Thus, complete tailoring of both circular and linear properties can be achieved through an appropriate choice of laser parameters. From a practical viewpoint, one has to take also into account the optical loss (due to absorption and scattering). Our structures exhibited a typical 74% transmission at 550 nm.

In summary, we propose a multilayer strategy for the fabrication of chiral waveplates with suppressed linear birefringence. Our theoretical model indicates the possibility of achieving large CB values accompanied by close-to-zero TLB ones. Experimentally, tailoring circular and linear properties is achieved by tuning the laser parameters (such as, the laser pulse energy). This work is believed to contribute to the study of fundamental light-matter interaction, as well as to provide new perspectives in laser manufacturing, especially in polarization control devices such as optical rotators and passive optical isolators.

Disclosures. The authors declare no conflicts of interest.

Data availability. Data is available upon reasonable requirements.

Funding. Agence Nationale pour la Recherche, FLAG-IR project (ANR-18-CE08-0004-01); Jiafeng Lu acknowledges the China Scholarship Council (CSC) for the funding No. 202006890077.

References

1. P. Zijlstra, J. W. M. Chon, and M. Gu, Nature **459**, 410 (2009).
2. J. K. Gansel, M. Thiel, M. S. Rill, M. Decker, K. Bade, V. Saile, G. Von Freymann, S. Linden, and M. Wegener, Science **325**, 1513 (2009).
3. H. Hübener, U. De Giovannini, C. Schäfer, J. Andberger, M. Ruggenthaler, J. Faist, and A. Rubio, Nat. Mater. **20**, 438 (2021).
4. R. Desmarchelier, M. Lancry, M. Gecevicius, M. Beresna, P. G. Kazansky, and B. Poumellec, Appl. Phys. Lett. **107**, 181111 (2015).
5. X. Wang, H. Yu, P. Li, Y. Zhang, Y. Wen, Y. Qiu, Z. Liu, Y. P. Li, and L. Liu, Opt. Laser Technol. **135**, 106687 (2021).
6. K. Sugioka and Y. Cheng, Light Sci. Appl. **3**, e149 (2014).
7. Y. Shimotsuma, P. G. Kazansky, J. Qiu, and K. Hirao, Phys. Rev. Lett. **91**, 247405 (2003).
8. M. Lancry, B. Poumellec, J. Canning, K. Cook, J. C. Poulin, and F. Brisset, Laser Photonics Rev. **7**, 953 (2013).
9. J. Lu, Y. Dai, Q. Li, Y. Zhang, C. Wang, F. Pang, T. Wang, and X. Zeng, Nanoscale **11**, 908 (2019).
10. Y. Shimotsuma, M. Sakakura, P. G. Kazansky, M. Beresna, J. Qiu, K. Miura, and K. Hirao, Adv. Mater. **22**, 4039 (2010).
11. Y. Shimotsuma, K. Miura, and H. Kazuyuki, Int. J. Appl. Glas. Sci. **4**, 182 (2013).
12. B. Poumellec, M. Lancry, R. Desmarchelier, E. Hervé, and B. Bourguignon, Light Sci. Appl. **5**, e16178 (2016).
13. J. Lu, J. Tian, B. Poumellec, E. Garcia-caurel, R. Ossikovski, X. Zeng, and M. Lancry, Light Sci. Appl. accepted, (2022).
14. J. Tian, R. Li, S. H. Yoo, B. Poumellec, E. Garcia-Caurel, R. Ossikovski, M. Stchakovsky, C. Eypert, J. Canning, and M. Lancry, OSA Contin. **2**, 1233 (2019).
15. R. Desmarchelier, M. Lancry, J. Tian, and B. Poumellec, Appl. Phys. Lett. **110**, 021112 (2017).
16. S. H. Yoo, R. Ossikovski, and E. Garcia-Caurel, Appl. Surf. Sci. **421**, 870 (2017).
17. R. Ossikovski, Opt. Lett. **36**, 2330 (2011).
18. R. Ossikovski and O. Arteaga, Opt. Lett. **39**, 4470 (2014).
19. Y. Dai, J. Ye, M. Gong, X. Ye, X. Yan, G. Ma, and J. Qiu, Opt. Express **22**, 28500 (2014).